



OPEN

Cobalt monoxide-doped porous graphitic carbon microspheres for supercapacitor application

Zheng-Chun Yang¹, Chun-Hua Tang¹, Yu Zhang¹, Hao Gong¹, Xu Li² & John Wang¹¹Department of Materials Science and Engineering, National University of Singapore, Blk EA, #03-09, 9 Engineering Drive 1, Singapore 117576, ²Institute of Materials Research and Engineering (IMRE), The Agency for Science, Technology and Research (A-STAR), 3, Research Link, Singapore 117602.

A novel design and facile synthesis process for carbon based hybrid materials, i.e., cobalt monoxide (CoO)-doped graphitic porous carbon microspheres (Co-GPCMs), have been developed. With the synthesis strategy, the mixture of cobalt gluconate, α -cyclodextrin and poly (ethylene oxide)₁₀₆-poly (propylene oxide)₇₀-poly (ethylene oxide)₁₀₆ is treated hydrothermally, followed by pyrolysis in argon. The resultant Co-GPCMs exhibits a porous carbon matrix with localized graphitic structure while CoO nanodots are embedded in the carbon frame. Thus, the Co-GPCMs effectively combine the electric double-layer capacitance and pseudo-capacitance when used as the electrode in supercapacitor, which lead to a higher operation voltage (1.6 V) and give rise to a significantly higher energy density. This study provides a new research strategy for electrode materials in high energy density supercapacitors.

Supercapacitors, which are also named as ultracapacitors or electrochemical capacitors, have attracted considerable attention due to their high power density, low cost and high efficiency¹⁻³. In recent years, they have been extensively investigated for energy storage, in attempts to improve their energy density and overall performance¹⁻³. In general, there are two main types of supercapacitors on the basis of energy storage process¹⁻³. The first type is the electric double-layer supercapacitors (EDLS), where the capacitance is generated from the electrostatic charges which are stored at the interface between electrode and electrolyte⁴. In the development of electrode materials with high surface specific area and controlled porosity for EDLS, carbon-based materials, such as activated carbon, carbon nanotubes, graphene, carbon film, carbon foam and mesoporous carbon, have been investigated⁵⁻¹⁰. They are among the most promising materials owing to their desirable physical and chemical behaviour and processing ability, including tuneable morphologies, controllable porosity, relatively inert surface electrochemistry, high electrical conductivity and low manufacturing cost⁵⁻¹¹. Since there is no electrochemical reaction between the electrode of carbon and electrolyte, the performance of EDLS is mainly dependent on the available surface area, pore size distribution, connectivity and electrical conductivity¹². In contrast, pseudo-supercapacitors are the other type of supercapacitors, which are built on the basis of the fast and reversible faradaic reactions between electrode materials and electrolytes¹³. There is faradaic current across the supercapacitor cell during the reversal processes of charging and discharging, which not only increases the specific capacitance but also extends the operation voltage of the supercapacitor¹⁴. Thus, transition metal (such as ruthenium, manganese, vanadium, tin, iron, nickel and cobalt) oxides and hydroxides with pseudo-capacitive behaviour are of great interest for the application as electrode materials in pseudo-supercapacitors¹⁵⁻²⁵. Although in recent years, a large number of studies have been made with the development of both types of supercapacitors with both theoretical understanding and practical fabrication made, the main challenges are still the low energy density and poor overall performance, which have to be tackled in order to widen the applications of supercapacitors^{1-3,26}. In order to improve the desperately wanted energy density, an effective approach is to increase the capacitance and operation voltage, since the energy density (E) is in theory related to both parameters, $E = 0.5CV^2$, where C (in farads) and V (in volts) are the capacitance and operation voltage, respectively^{3,27}. Therefore, electrode materials with the desirable physical and electrochemical performances are the key factors in leading to high energy density for supercapacitors²⁸. In particular, it would be of interest to effectively combine the double-layer capacitance and pseudo-capacitance by developing a hybrid type of electrode materials, where electric double-layers and faradaic capacitance can be realized concurrently to contribute to the high energy density and better overall performance²⁹.

SUBJECT AREAS:
POROUS MATERIALS
SYNTHESIS AND PROCESSING
NANOPARTICLES
BATTERIESReceived
31 May 2013Accepted
24 September 2013Published
11 October 2013Correspondence and
requests for materials
should be addressed to
X.L. (x.li@imre.a-star.
edu.sg) or Z.Y.
(g0801400@nus.edu.
sg)

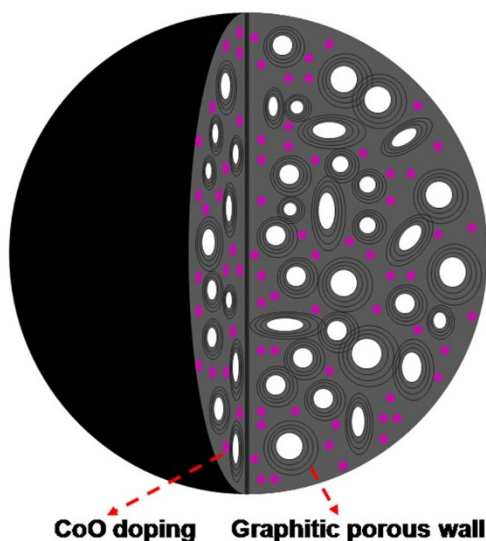


Figure 1 | Schematic representation of Co-GPCMs developed in the present study.

Herein, we report a novel design and facile synthesis process for carbon based hybrid materials, i.e., cobalt monoxide (CoO)-doped graphitic porous carbon microspheres (Co-GPCMs), as a promising electrode material in supercapacitors showing high energy density. As shown in Fig. 1, the desirable carbon microspheres would contain both nanopores (1–2 nm) and mesopores (5–50 nm), where the carbon wall exhibits the graphitic structure. For energy storage by EDLS, the porous structure of carbon microspheres would provide the wanted interfaces for electrostatic charge accumulation, while the graphitic carbon wall could enhance the electric conductivity³⁰. Moreover, CoO as a transitional metal oxide offers the potential of pseudo-supercapacitors²⁵. The hybrid electrode is expected to be electrochemically active, enabling the reaction with the electrolyte by fast and reversible faradaic reactions to enhance the operation voltage³¹. This would effectively combine the EDLS of carbon and pseudo-supercapacitors of CoO, leading to an improvement in energy density. The designed Co-GPCMs are prepared by a facile synthesis process, conducted under controlled hydrothermal condition, where the mixture of cobalt gluconate (Co-gluconate), α -cyclodextrin (α -CD) and poly (ethylene oxide)₁₀₆-poly (propylene oxide)₇₀-poly (ethylene oxide)₁₀₆ (F127) is treated hydrothermally, followed by pyrolysis process in argon (Ar). As detailed in the results and discussion below, the resultant Co-GPCMs is demonstrated promising as an electrode material in supercapacitors.

Results

The scanning electron microscopy (SEM) and transmission electron microscopy (TEM) images of the microspheres derived from the hydrothermal treatment of Co-gluconate and α -CD in the presence of F127 are shown in Fig. 2 (a) and (b), where one can see their morphologies and inner structures. The hydrothermal treatment of Co-gluconate and α -CD in the presence of F127 at 200 °C for 6 h lead to a spherical structure with average size of 1464 nm. In addition, from the TEM image shown in Fig. 2 (b), the carbon microspheres are solid without cavity inside the carbon frame. In contrast, upon pyrolysis treatment of the as-prepared carbon microspheres in Ar gas at 900 °C for 3 h, a graphitic porous carbon structure is established for Co-GPCMs, as shown in Fig. 2 (c) and (d). From the SEM image in Fig. 2 (c), the Co-GPCMs are spherical in morphology with an average size of ~1200 nm. Moreover, the surface of these Co-GPCMs appears rough, which is apparently due to the decomposition of F127 by pyrolysis³². Indeed the decomposition of F127 by pyrolysis treatment is confirmed by the shrinkage in the average

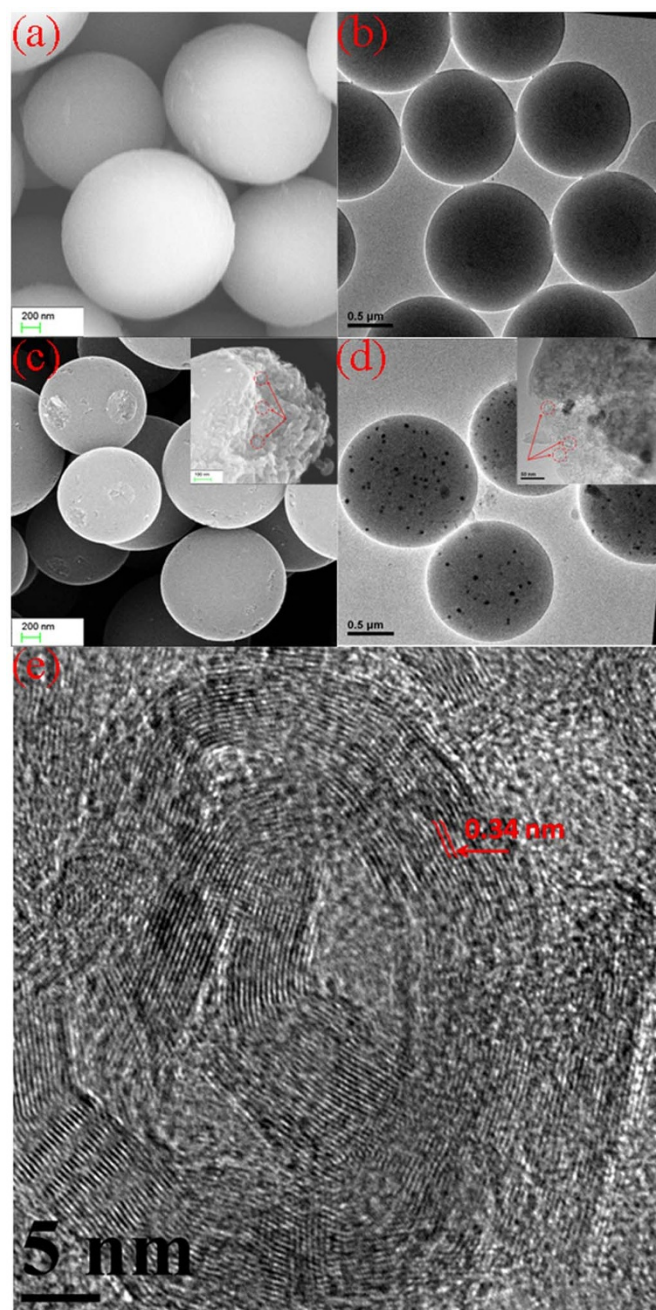


Figure 2 | SEM (a), and TEM (b) images of carbon microspheres synthesized by hydrothermal treatment of Co-gluconate and α -CD together in the presence of F127. SEM (c) and TEM (d) images of Co-GPCMs after pyrolysis treatment, where their fracture surfaces are shown in inset of (c) and (d). High resolution TEM (e) image of the fracture section of Co-GPCMs.

microsphere size, which is indicated by the change in size distribution histogram before and after pyrolysis (see Supplementary Fig. S1 online). As a result, upon pyrolysis, there is a visible porous structure established in the carbon frame, which is further confirmed by SEM and TEM images showing their fracture surface (inset in Fig. 2 (c) and (d)). In addition, the TEM image shown in Supplementary Fig. S2 confirms the presence of pores of varying sizes inside the Co-GPCMs. As shown in Fig. 2 (e), which is a high resolution TEM image of an individual pore inside Co-GPCMs, it appears to consist of crystallized carbon, which is in close match with the (002) lattice spacing of disordered graphite³³. In addition, as shown in Fig. 2 (d), the black dots embedded in the carbon spheres are Co in

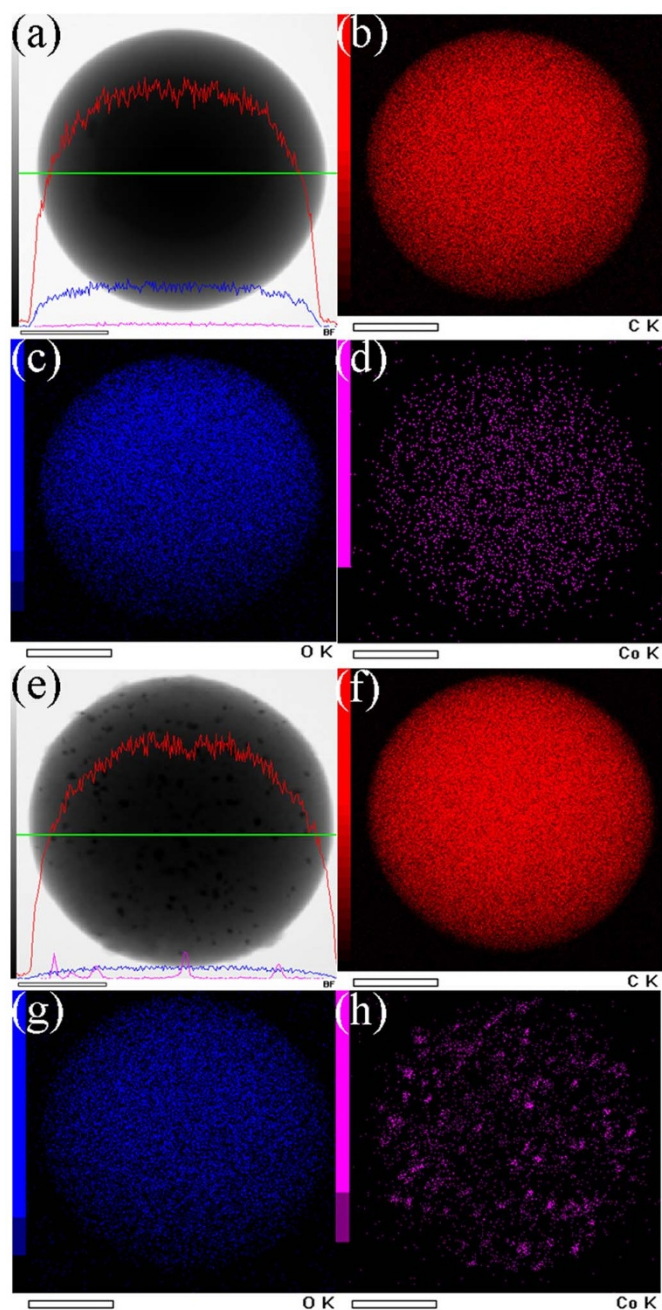


Figure 3 | STEM-EDX line analysis of individual carbon microspheres synthesized by hydrothermal treatment of Co-gluconate and α -CD together with F127 (a), and the corresponding element mapping result (b–d). STEM-EDX line analysis of individual carbon microspheres of Co-GPCMs (e) and the corresponding element mapping result (f–h). The red, blue and purple colour represents C, O and Co element, respectively. The scale bar is 500 nm.

composition, which is further confirmed by scanning TEM-energy dispersive X-ray spectroscopy (STEM-EDX) line analysis and element mapping as shown in Fig. 3.

As shown in Fig. 3, the carbon microspheres contain rather uniformly distributed Co element, as confirmed by the STEM-EDX line analysis (Fig. 3 (a)) and the corresponding Co element mapping (Fig. 3 (d)). At the hydrothermal temperature of 200°C, α -CD is converted to carbon while the dissolved Co salt is wrapped in the carbon matrix, which is assisted by the hydrogen bonding between Co-gluconate with α -CD and F127³⁴. Upon pyrolysis, the soft template of F127 is decomposed to generate a porous structure inside the

Co-GPCMs. The structure change of F127 is demonstrated by Fourier transform infrared (FTIR) spectrometry (see Supplementary Fig. S3 online), where the characteristic FTIR peaks of F127 have disappeared in the FTIR spectrum of Co-GPCMs. In addition, since Co-gluconate is an inorganic salt, which would be converted to Co-based nanodots at the high temperature of pyrolysis treatment, Co is known to play a key function of acting as a catalyst for forming graphitic carbon³⁵. The conversion of Co-gluconate to Co-based nanodots distributed in the Co-GPCMs is confirmed by the STEM-EDX line analysis (Fig. 3 (e)) and the corresponding Co element mapping (Fig. 3 (h)). To further understand the crystal structure and porous distribution in Co-GPCMs, X-ray diffraction (XRD), Raman spectrum and Brunauer-Emmett-Teller (BET) analysis are conducted, which are shown in Fig. 4.

From the XRD phase analysis, which is shown in Fig. 4 (a), crystallites of both carbon and Co-based nanodots in Co-GPCMs can be identified. Obviously, Fig. 4 (a) shows a typical characteristic XRD pattern of graphitic carbon (labelled by + in Fig. 4 (a)), which exhibits peaks at 2θ of 26°, 44°, 54° and 77°. These peaks are assigned to the (002), (101), (004) and (110) planes of the graphitic carbon frame, respectively (JCPDS file number 41-1487)³⁶. In addition, the presence of the sharp (002) diffraction peak indicates that the Co-GPCMs exhibits a highly ordered graphitic structure, which corresponds well to the result of TEM studies in Fig. 2³⁶. The crystalline phase of Co-based nanodots is identified by the XRD peaks (labelled by * in Fig. 4 (a)) at 2θ angles of 37°, 42° and 62°, which represent the (111), (200) and (220) diffractions of CoO (JCPDS file number 43-1004)³⁷. The amount of CoO retained in Co-GPCMs is measured to be 4.2 wt.% by Inductively Coupled Plasma (ICP) analysis. Since there is a rather small amount of CoO in the Co-GPCMs, which is further confirmed by the STEM-EDX line analysis (Fig. 3 (e)) and the EDX spectrum (see Supplementary Fig. S4 online), the presence of CoO nanodots is not as obvious as that of the graphitic carbon. The phase structures of graphitic carbon and CoO nanodots embedded in the microspheres are further studied by using Raman spectrometer, the result of which is shown in Fig. 4 (b). As labelled by + in Fig. 4 (b), the peaks centred at 1338, 1593, 2694 and 2922 cm^{-1} are the representative bands of graphitic carbon³⁸. Among them, the three intense peaks at 1338, 1593 and 2694 cm^{-1} are assigned to the defect, the breath mode of graphite lattice and the 2nd order band of graphite, respectively³⁹. Moreover, the peak centred at 2694 cm^{-1} indicates the presence of sp^3 C-H and C-H₂ groups in the Co-GPCMs⁴⁰. In addition, the presence of CoO nanodots in Co-GPCMs is further confirmed by the corresponding peak at 468 and 672 cm^{-1} (labelled by * in Fig. 4 (b))⁴¹. Thus, the result of Raman spectroscopy agrees well with the TEM and XRD studies. By comparison, in the Raman spectra and XRD traces of the carbon microspheres synthesized by hydrothermal treatment of Co-gluconate and α -CD in the presence of F127 at 200°C for 6 h (see Supplementary Fig. S5 online), there is no clear indication for the characteristic peaks of ordered graphite and crystallized CoO. As shown in Fig. S5 (a), the Raman spectra of the carbon microspheres before pyrolysis treatment exhibits the characteristic peaks at 1389 and 1583 cm^{-1} . The peak at 1583 cm^{-1} is broader than the typical G band of disordered graphite, indicating that there are aromatic and olefinic molecules co-existing in the carbon microspheres³². The existence of sp^2 carbon atoms pairs is demonstrated by the broad XRD peak at 26° in Fig. S5 (b). During the pyrolysis, graphitic carbon is formed from these aromatic carbon structures by the catalyst effect of Co element inside the carbon microspheres³⁵. Since CoO is formed when the Co-based compound is annealed at 900°C, the existence of CoO in the graphitic porous carbon frame is apparently due to the conversion of Co-gluconate at the pyrolysis temperature as O is present in the α -CD and F127³⁷. The porous structure of Co-GPCMs is further studied by BET measurement using nitrogen (N_2). As shown in Fig. S5 (c), there is negligible N_2 adsorption occurring over the relative pressure range

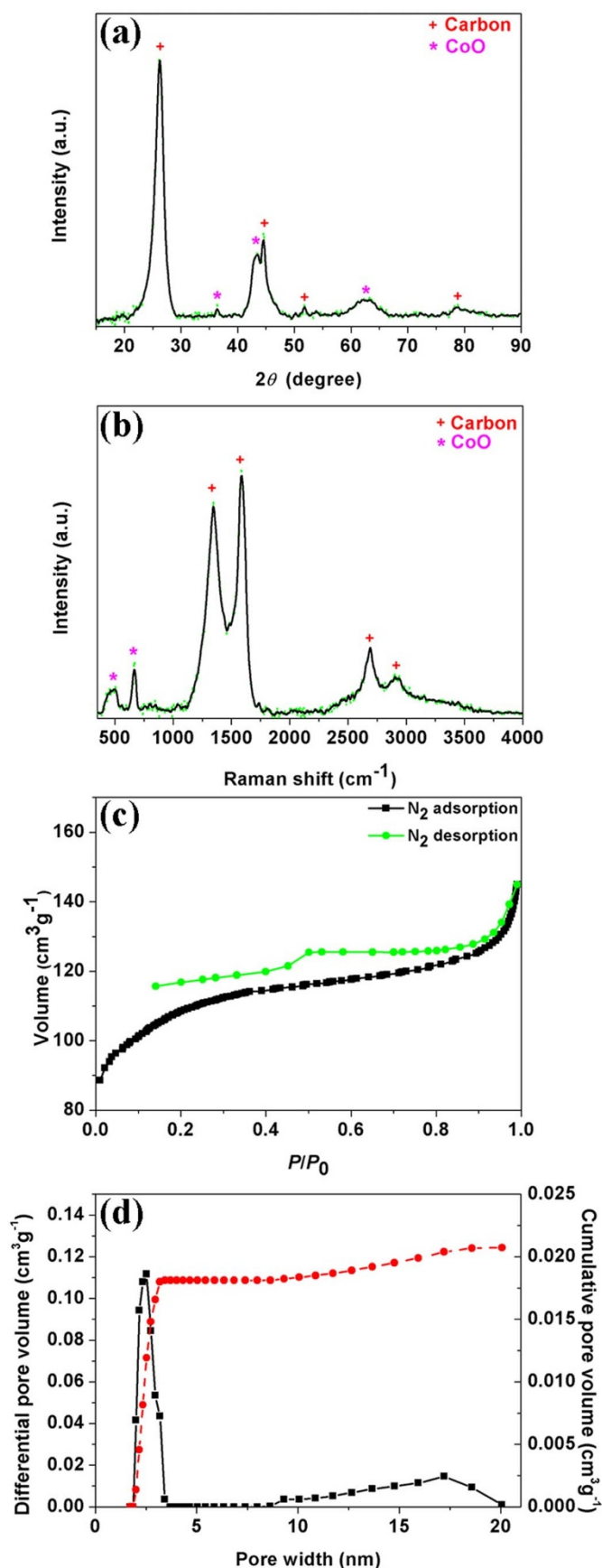


Figure 4 | XRD (a), Raman spectrum (b), N_2 adsorption/desorption isotherm (c) and NLDFT pore size distribution (d) of Co-GPCMs.

(P/P_0) of 0–0.9 indicating a nonporous character for the carbon microspheres before pyrolysis, where the specific surface area calculated from the BET result is quite small, i.e., $7.2 \text{ m}^2\text{g}^{-1}$. In contrast, the porous structure of the carbon frame of Co-GPCMs generated by pyrolysis treatment is demonstrated, as shown in Fig. 4 (c) and (d). The N_2 adsorption/desorption isotherms for Co-GPCMs (Fig. 4 (c)) demonstrate that both nanopores and mesopores are present in the Co-GPCMs with a total BET surface area of $381 \text{ m}^2\text{g}^{-1}$. As shown in the N_2 adsorption curve, the linear increase of N_2 uptake at low pressure range, which is $P/P_0 = 0.06\text{--}0.2$, indicates a monolayer gas adsorption inside the pores^{32,42}. When approaching the full filling of pores, the adsorption curve of N_2 shows a near plateau at $P/P_0 = 0.2\text{--}0.9$, which suggests the presence of nanopores (60% in t-plot pore volume) together with some mesopores. This is further confirmed by the pore size distribution peaked at 2.5 nm (Fig. 4 (d)) with a differential pore volume of $0.11 \text{ cm}^3\text{g}^{-1}$, which is calculated by the nonlocal density functional theory (NLDFT) method. Moreover, the sharp increase in the N_2 adsorption curve at $P/P_0 = 0.9\text{--}1.0$ corresponds to the inter-particle voids^{32,42}. The aggregates of platy particles make the non-closing hysteresis loops at $P/P_0 = 0.4\text{--}1.0$ while the ink-bottle type of pores leads the sudden closure at $P/P_0 = 0.4$ in the N_2 desorption branch⁴³.

Discussion

On the basis of the characterization results of Co-GPCMs, there are both nanopores and mesopores inside the carbon microspheres with localized graphitic structure, which would benefit the specific surface area and electrical conductivity. In addition, the presence of CoO nanodots in the carbon matrix could give rise to pseudo-capacitance. The performance of Co-GPCMs as electrode materials in supercapacitors is evaluated by cyclic voltammetry (CV) and galvanostatic charge-discharge measurement (Fig. 5) in 6 M potassium hydroxide (KOH) aqueous electrolyte. As shown in Fig. 5 (a) and (b), the quasi-rectangular voltammogram shape and symmetric linear galvanostatic charge-discharge profile show the typical electrochemical behaviour of carbon-based materials within the operation voltage of $-1.2\text{--}0 \text{ V}$, which implies that the Co-GPCMs exhibits excellent capacitive behaviour and electrochemical reversibility for EDLS^{36,44}. In addition, the presence of pseudo-capacitance is demonstrated in Fig. 5 (c) and (d) with a typical CV and galvanostatic charge-discharge shape for CoO, which indicates the faradaic reactions, $\text{CoO} + \text{OH}^- \leftrightarrow \text{CoOOH} + e^-$ and $\text{CoOOH} + \text{OH}^- \leftrightarrow \text{CoO}_2 + \text{H}_2\text{O} + e^-$, taking place within the operation voltage of $0\text{--}0.4 \text{ V}$ ²⁵. Further studies with the working electrode made of Co-GPCMs within the operation voltage of $-1.2\text{--}0.4 \text{ V}$, which is shown in Fig. 5 (e) and (f), show that the supercapacitor working electrode exhibits both electric double-layer capacitance and pseudo-capacitance in 6 M KOH aqueous electrolyte. Thus, the overall operation voltage of the supercapacitor working electrode made of Co-GPCMs is 1.6 V in 6 M KOH aqueous electrolyte, which is higher than the typical porous carbon and Co based materials^{1–3,25,45}. Moreover, the specific capacitance for the working electrode made of Co-GPCMs (Fig. 5 (g)) is 194, 92 and 191 Fg^{-1} within the operation voltage of $-1.2\text{--}0$, $0\text{--}0.4$ and $-1.2\text{--}0.4 \text{ V}$, respectively, at the current density of 0.1 Ag^{-1} . These results indicate that the overall specific capacitance of Co-GPCMs is at least comparable to the best porous carbon materials, while doping CoO nanodots into the carbon matrix gives rise to an extension of operation voltage. For comparison purpose, a working electrode is made of carbon spheres synthesized from α -CD and F127 without Co-gluconate by following the same experimental procedure (see Supplementary Fig. S6, and S7 online). As shown in Fig. S6, when Co-gluconate is not added, the carbon spheres do not contain any graphitic porous structure. The electrochemical performance is expectedly similar with that of a conventional carbon material (see Supplementary Fig. S7 online), where quasi-rectangular shape of voltammogram (see Supplementary Fig. S7 (a) (b) and (c) online)

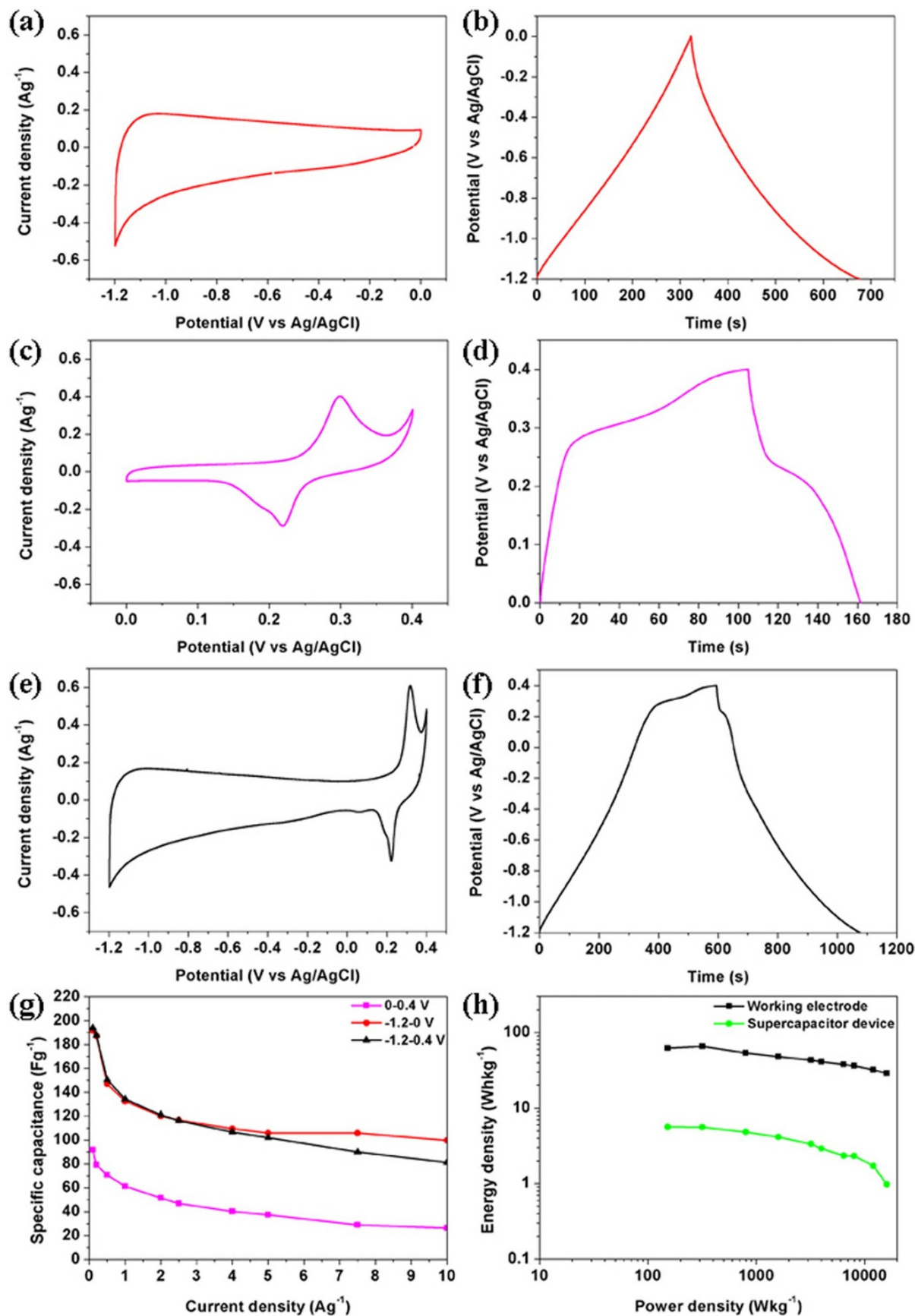


Figure 5 | Electrochemical performance of Co-GPCMs as working supercapacitor electrode: CV curve at a scan rate of 1 mVs^{-1} within the operation voltage of $-1.2\text{--}0 \text{ V}$ (a), $0\text{--}0.4 \text{ V}$ (c) and $-1.2\text{--}0.4 \text{ V}$ (e) in the three electrode configuration; galvanostatic charge-discharge at a current density of 0.5 Ag^{-1} within the operation voltage of $-1.2\text{--}0 \text{ V}$ (b), $0\text{--}0.4 \text{ V}$ (d) and $-1.2\text{--}0.4 \text{ V}$ (f) in the three electrode configuration; variation of specific capacitance against different current densities within the operation voltage of $-1.2\text{--}0 \text{ V}$, $0\text{--}0.4 \text{ V}$ and $-1.2\text{--}0.4 \text{ V}$ in the three electrode configuration (g) and the ragone plot of the supercapacitor working electrode and device in three and two electrode configurations, respectively (h).



and symmetric linear galvanostatic charge-discharge profile (see Supplementary Fig. S7 (c) online) are shown. The operation voltage is only from -1.0 to 0 V, within which the specific capacitance is 188 and 148 Fg^{-1} at the current density of 0.1 Ag^{-1} and scan rate of 1 mVs^{-1} , respectively (see Supplementary Fig. S7 (d) and (e) online). In addition, the establishment of graphitic carbon structure in Co-GPCMs provides a higher conductivity, which is confirmed by the internal resistance calculated from the plot of IR drop (see Supplementary Fig. S8 online). The equivalent series resistance (ESR) of Co-GPCMs is calculated to be $0.03069 \text{ }\Omega\text{g}$. The specific capacitance of the working electrode made of Co-GPCMs could retain 40% with the increase in current density from 0.1 to 10 Ag^{-1} (Fig. 5 (g)), while the shape of CV is still maintained with the increase in scan rate from 1 to 100 mVs^{-1} (see Supplementary Fig. S9 online). Furthermore, from Fig. S9 (a)–(c), the specific capacitance of the working electrode made of Co-GPCMs is seen to retain 55% with the increase in scan rate, which shows a good rate capability. This highlights that the working electrode would be suitable for fast charge-discharge and high scan rate operations within the potential window of $1.6 \text{ V}^{30,46}$. The high operation voltage (1.6 V) of the working electrode made of Co-GPCMs could therefore generate an improved high energy density for supercapacitors. In order to understand the performance for energy density, the Ragone plot (Fig. 5 (h)) is calculated based on the CV and galvanostatic charge-discharge results, where one sees an energy density of 62 Whkg^{-1} at a power density of 152 Wkg^{-1} . It maintains 29 Whkg^{-1} at a power density of 1.6 kWkg^{-1} in the three electrode system. With a symmetric two working electrode system, the energy density is 5.6 Whkg^{-1} at a power density of 152 Wkg^{-1} while maintaining 1.0 Whkg^{-1} at a power density of 1.6 kWkg^{-1} . In contrast, when there was no CoO doping in the carbon spheres, the overall energy density was much lower than that of Co-GPCMs (see Supplementary Fig. S10 online). In addition, the working electrode made of Co-GPCMs demonstrates similar electrochemical behaviour by using either Ag/AgCl or saturated calomel electrode (SCE) reference electrode (see Supplementary Fig. S11 online). As shown in Fig. S11, the supercapacitor working electrode shows both electric double-layer capacitance and pseudo-capacitance performance by using SCE as the reference electrode. The specific capacitance for the working electrode made of Co-GPCMs is 210 , 97 and 210 Fg^{-1} within the operation voltage of -1.2 – 0 , 0 – 0.4 and -1.2 – 0.4 V , respectively, at the current density of 0.1 Ag^{-1} by using SCE as the reference electrode. The working electrode could retain 47% of the specific capacitance with the increase in current density from 0.1 to 10 Ag^{-1} , while the CV shape is still maintained with the increase in scan rate from 1 to 100 mVs^{-1} . 54% of the specific capacitance could be retained with the increase in scan rate, demonstrating a good rate capability of the working electrode by using SCE as the reference electrode. From the CV and galvanostatic charge-discharge results in Fig. S11, one can see an energy density of 68 Whkg^{-1} at a power density of 152 Wkg^{-1} . It maintains an energy density of 36 Whkg^{-1} at the power density of 1.6 kWkg^{-1} in the SCE reference electrode system. These data demonstrate the excellent capacitive performance of Co-GPCMs with the aqueous electrolyte. Concerning the cyclic retention, the working electrode made of Co-GPCMs could retain 90% of the specific capacitance after 1500 cycles of measurement. It could retain 22% after 5000 cycles of measurements (see Supplementary Fig. S12 online), the exact cause for which is subject to further investigation.

In summary, a novel design and facile synthesis process have been developed for hybrid-type carbon microspheres, which exhibit a graphitic porous structure. The Co-GPCMs are successfully realized by the hydrothermal treatment of Co-gluconate and α -CD in the presence of F127, followed by pyrolysis at high temperature in Ar. The Co-GPCMs consists of a porous carbon matrix with localized graphitic structure while CoO nanodots are embedded in the carbon frame. The hybrid structure is aimed at effectively combining the

electric double-layer capacitance and pseudo-capacitance, which has been successfully demonstrated when used as the electrode material in supercapacitors. The combination of EDLS, which is generated by the porous graphitic carbon, and pseudo-supercapacitors, which is generated by CoO, leads to a high operation voltage (1.6 V), which gives rise to a high energy density.

Methods

Materials. Co-gluconate and F127 were purchased from Sigma-Aldrich Company. α -CD was purchased from Tokyo Chemical Industry Company. All chemicals were used without further purification. For fabrication of working electrode, carbon black was purchased from CABOT Company (VULCAN[®]XC72). Polytetrafluoroethylene was purchased from Sigma-Aldrich Company (60 wt.% in H_2O). Ni foam was purchased from LATECH Company (>99% Ni, 90–98% volumetric porosity).

Synthesis of Co-GPCMs. Co-GPCMs were synthesised via hydrothermal treatment route followed by pyrolysis. Firstly, 300 mg F127 was dissolved in 20 mL deionized (DI) water. 49 mg of Co-gluconate dissolved in 10 mL DI water was then injected into the solution of F127 under stirring at 700 rpm . After that, 600 mg of α -CD dissolved in 10 mL DI water was injected into the mixed solution of F127 and Co-gluconate under stirring at 700 rpm . The mixed solution was further stirred overnight and then transferred into a Teflon sealed autoclave tube. Upon hydrothermal treatment at 200°C for 6 h , the clear solution turned into black in appearance. The black product was then collected by centrifugation at 9000 rpm for 30 min , and then washed by DI water three times. After washing, the black precipitates were re-dispersed in DI water and freeze dried for two days to obtain the black powder. Finally, the dried powder was further pyrolyzed in a tube furnace at 900°C for 3 h under Ar gas protection.

Characterization. The morphology and phase structure of the products were studied by using SEM (ZEISS SUPRA 40) and TEM (CM 300 FEG-Philips). To study their fracture surface, the as-synthesized Co-GPCMs powders were frozen by liquid N_2 and grinded to get fracture surface. The STEM-EDX line analysis and elemental mapping were conducted by using TEM (JEOL 2100). FTIR spectra were acquired by using Perkin Elmer FT-IR 2000 spectrometer, where the sample was prepared by pressing the mixture of the sample powder and potassium bromide into a thin disk. XRD phase analysis was conducted by using Bruker D8 XRD which is equipped with $\text{Cu K}\alpha$ radiation ($\lambda = 0.15418 \text{ nm}$). Raman spectra were acquired by using RENISHAW Raman Microscope with 514 nm laser radiation source. N_2 adsorption and desorption isotherms were measured at -196°C by using a Micromeritics ASAP 2020 system. In addition, the surface area was determined by the BET method and the pore size distribution was calculated using the NLDFT method. The amount of CoO in carbon spheres was determined by ICP analysis using Perkin Elmer Dual-view Optima 5300 DV ICP-OES system.

Electrochemical performance evaluation of Co-GPCMs. Electrochemical performances of the Co-GPCMs as supercapacitor working electrode materials were investigated using a Solartron Electrochemical System SI 1287. The working electrode was fabricated by coating the viscous slurry of Co-GPCMs (80 wt.%), carbon black (10 wt.%), and polytetrafluoroethylene (10 wt.%) in ethanol onto a Ni foam of 2.25 cm^2 in area and 1 mm in thickness. After drying in a vacuum oven at 120°C for 12 h , the coated Ni foam was uniaxially pressed at a pressure of 49 MPa to enhance the adhesion between the active materials (18.7 mg) and the Ni foam. A series of electrochemical tests were made with the working electrode, including the CV and galvanostatic charge-discharge by using 6 M KOH aqueous solution as the electrolyte, which was purged with N_2 , within the operation voltage of -1.2 – 0 , 0 – 0.4 and -1.2 – 0.4 V . The fabrication procedure of working electrode for carbon spheres made from α -CD and F127 is the same as that described above. In the three electrode system, Pt foil was used as the counter electrode, while Ag/AgCl or SCE was used as reference electrode. In the two electrode system, two working electrodes with the same active loading mass were applied.

1. Wang, G., Zhang, L. & Zhang, J. A review of electrode materials for electrochemical supercapacitors. *Chem. Soc. Rev.* **41**, 797–828 (2012).
2. Simon, P. & Gogotsi, Y. Materials for electrochemical capacitors. *Nat. Mater.* **7**, 845–854 (2008).
3. Zhang, L. & Zhao, X. S. Carbon-based materials as supercapacitor electrodes. *Chem. Soc. Rev.* **38**, 2520–2531 (2009).
4. Kötz, R. & Carlen, M. Principles and applications of electrochemical capacitors. *Electrochim. Acta.* **45**, 2483–3498 (2000).
5. Raymundo-Pinero, E., Leroux, F. & Beguin, F. A High-Performance Carbon for Supercapacitors Obtained by Carbonization of a Seaweed Biopolymer. *Adv. Mater.* **18**, 1877–1882 (2006).
6. Futaba, D. N. *et al.* Shape-engineerable and highly densely packed single-walled carbon nanotubes and their application as super-capacitor electrodes. *Nat. Mater.* **5**, 987–994 (2006).
7. Sheng, K., Sun, Y., Li, C., Yuan, W. & Shi, G. Ultrahigh-rate supercapacitors based on electrochemically reduced graphene oxide for ac line-filtering. *Sci. Rep.* **2**, 247(1)–247(5) (2012).



8. Zhang, L. *et al.* Porous 3D graphene-based bulk materials with exceptional high surface area and excellent conductivity for supercapacitors. *Sci. Rep.* **3**, 1408(1)–1408(9) (2013).
9. Jung, H. Y., Karimi, M. B., Hahm, M. G., Ajayan, P. M. & Jung, Y. J. Transparent, flexible supercapacitors from nano-engineered carbon films. *Sci. Rep.* **2**, 773(1)–773(5) (2012).
10. Lee, J., Kim, J. & Hyeon, T. Recent Progress in the Synthesis of Porous Carbon Materials. *Adv. Mater.* **18**, 2073–2094 (2006).
11. Li, Q. *et al.* Facile synthesis of activated carbon/carbon nanotubes compound for supercapacitor application. *Chem. Eng. J.* **156**, 500–504 (2010).
12. Ghosh, A. & Lee, Y. H. Carbon-Based Electrochemical Capacitors. *ChemSusChem* **5**, 480–499 (2012).
13. Liu, C., Li, F., Ma, L.-P. & Cheng, H.-M. Advanced Materials for Energy Storage. *Adv. Mater.* **22**, E28–E62 (2010).
14. Conway, B. E., Birss, V. & Wojtowicz, J. The role and utilization of pseudocapacitance for energy storage by supercapacitors. *J. Power Sources* **66**, 1–14 (1997).
15. Kim, I. H. & Kim, K. B. Electrochemical Characterization of Hydrous Ruthenium Oxide Thin-Film Electrodes for Electrochemical Capacitor Applications. *J. Electrochem. Soc.* **153**, A383–A389 (2006).
16. Wang, Z., Guo, R., Ding, L., Tong, Y. & Li, G. Controllable Template-Assisted Electrodeposition of Single- and Multi-Walled Nanotube Arrays for Electrochemical Energy Storage. *Sci. Rep.* **3**, 1204(1)–1204(8) (2013).
17. Lee, H. Y. & Goodenough, J. B. Ideal Supercapacitor Behavior of Amorphous $V_2O_5 \cdot nH_2O$ in Potassium Chloride (KCl) Aqueous Solution. *J. Solid State Chem.* **148**, 81–84 (1999).
18. Hwang, S. W. & Hyun, S. H. Synthesis and characterization of tin oxide/carbon aerogel composite electrodes for electrochemical supercapacitors. *J. Power Sources* **172**, 451–459 (2007).
19. Zhao, X., Johnston, C. & Grant, P. S. A novel hybrid supercapacitor with a carbon nanotube cathode and an iron oxide/carbon nanotube composite anode. *J. Mater. Chem.* **19**, 8755–8760 (2009).
20. Chen, J., Huang, K. & Liu, S. Hydrothermal preparation of octadecahedron Fe_3O_4 thin film for use in an electrochemical supercapacitor. *Electrochim. Acta.* **55**, 1–5 (2009).
21. Liu, K. C. & Anderson, M. A. Porous Nickel Oxide/Nickel Films for Electrochemical Capacitors. *J. Electrochem. Soc.* **143**, 124–130 (1996).
22. Lang, J. W. *et al.* A facile approach to the preparation of loose-packed $Ni(OH)_2$ nanoflake materials for electrochemical capacitors. *J. Solid State Electrochem.* **13**, 333–340 (2009).
23. Wei, T. Y., Chen, C. H., Chang, K. H., Lu, S. Y. & Hu, C. C. Cobalt Oxide Aerogels of Ideal Supercapacitive Properties Prepared with an Epoxide Synthetic Route. *Chem. Mater.* **21**, 3228–3233 (2009).
24. Cao, L., Xu, F., Liang, Y. Y. & Li, H. L. Diamond Nanorods from Carbon Nanotubes. *Adv. Mater.* **16**, 1853–1857 (2004).
25. Guan, C. *et al.* Hybrid structure of cobalt monoxide nanowire @ nickel hydroxidenitrate nanoflake aligned on nickel foam for high-rate supercapacitor. *Energy Environ. Sci.* **4**, 4496–4499 (2011).
26. Thounthong, P., Chankag, V., Sethakul, P., Davat, B. & Hinaje, M. Comparative Study of Fuel-Cell Vehicle Hybridization with Battery or Supercapacitor Storage Device. *IEEE Trans. Veh. Technol.* **58**, 3892–3940 (2009).
27. Pan, H., Li, J. & Feng, Y. Carbon Nanotubes for Supercapacitor. *Nanoscale Res. Lett.* **5**, 654–668 (2010).
28. Aricò, A. S., Bruce, P., Scrosati, B., Tarascon, J. & Chalkwijk, W. V. Nanostructured materials for advanced energy conversion and storage devices. *Nat. Mater.* **4**, 366–377 (2005).
29. Jiang, H., Ma, J. & Li, C. Mesoporous Carbon Incorporated Metal Oxide Nanomaterials as Supercapacitor Electrodes. *Adv. Mater.* **24**, 4197–4202 (2012).
30. Wang, D., Li, F., Liu, M., Lu, G. Q. & Cheng, H.-M. 3D Aperiodic Hierarchical Porous Graphitic Carbon Material for High-Rate Electrochemical Capacitive Energy Storage. *Angew. Chem. Int. Ed.* **47**, 373–376 (2008).
31. Wang, H. *et al.* Preparation of reduced graphene oxide/cobalt oxide composites and their enhanced capacitive behaviors by homogeneous incorporation of reduced graphene oxide sheets in cobalt oxide matrix. *Mater. Chem. Phys.* **130**, 672–679 (2011).
32. Yang, Z. *et al.* Hollow carbon nanoparticles of tunable size and wall thickness by hydrothermal treatment of α -cyclodextrin templated by F127 block copolymers. *Chem. Mater.* **25**, 704–710 (2013).
33. Bourlino, A. B. *et al.* Photoluminescent Carbogenic Dots. *Chem. Mater.* **20**, 4539–4541 (2008).
34. Dai, M., Song, L., LaBelle, J. T. & Vogt, B. D. Ordered Mesoporous Carbon Composite Films Containing Cobalt Oxide and Vanadia for Electrochemical Applications. *Chem. Mater.* **23**, 2869–2878 (2011).
35. Sevilla, M., Martínez-de Lecea, C. S., Valdés-Solis, T., Morallón, E. & Fuentès, A. B. Solid-phase synthesis of graphitic carbon nanostructures from iron and cobalt gluconates and their utilization as electrocatalyst supports. *Phys. Chem. Chem. Phys.* **10**, 1433–1442 (2008).
36. Wang, Z. *et al.* Co-gelation synthesis of porous graphitic carbons with high surface area and their applications. *Carbon* **49**, 161–169 (2011).
37. Al-Tuwirqi, R. M. *et al.* Synthesis and physical properties of mixed Co_3O_4/CoO nanorods by microwave hydrothermal technique. *Superlattices Microstruct.* **50**, 437–448 (2011).
38. Perraki, M., Proyer, A., Mposkos, E., Kaindl, R. & Hoinkes, G. Raman microspectroscopy on diamond, graphite and other carbon polymorphs from the ultrahigh-pressure metamorphic Kimi Complex of the Rhodope Metamorphic Province, NE Greece. *Earth. Planet. Sci. Lett.* **241**, 672–685 (2006).
39. Ferrari, A. C. *et al.* Raman Spectrum of Graphene and Graphene Layers. *Phys. Rev. Lett.* **97**, 187401(1)–187401(4) (2006).
40. Ferrari, A. C. & Robertson, J. Resonant Raman spectroscopy of disordered, amorphous, and diamondlike carbon. *Phys. Rev. B* **64**, 075414(1)–075414(13) (2001).
41. Choi, H. C., Jung, Y. M., Noda, I. & Kim, S. B. A Study of the Mechanism of the Electrochemical Reaction of Lithium with CoO by Two-Dimensional Soft X-ray Absorption Spectroscopy (2D XAS), 2D Raman, and 2D Heterospectral XAS-Raman Correlation Analysis. *J. Phys. Chem. B* **107**, 5806–5811 (2003).
42. Kubo, S., White, R. J., Yoshizawa, N., Antonietti, M. & Titirici, M. M. Ordered Carbohydrate-Derived Porous Carbons. *Chem. Mater.* **23**, 4882–4885 (2011).
43. Katcho, N. A. *et al.* Carbon Hollow Nanospheres from Chlorination of Ferrocene. *Chem. Mater.* **19**, 2304–2309 (2007).
44. Pan, H., Poh, C. K., Feng, Y. P. & Lin, J. Supercapacitor Electrodes from Tubes-in-Tube Carbon Nanostructures. *Chem. Mater.* **19**, 6120–6125 (2007).
45. Miller, J. R. & Simon, P. Electrochemical Capacitors for Energy Management. *Science* **321**, 651–652 (2008).
46. Xia, K., Gao, Q., Jiang, J. & Hu, J. Hierarchical porous carbons with controlled micropores and mesopores for supercapacitor electrode materials. *Carbon* **46**, 1718–1726 (2008).

Acknowledgments

This work is supported by the Agency for Science, Technology and Research (A-Star, Singapore), Grant number: 1121202013, conducted at the National University of Singapore.

Author contributions

Z.Y. designed and carried out the experiments. C.T. and H.G. supervised the electrochemical performance characterization. Y.Z. contributed the BET analysis. X.L. and J.W. supervised the project. Z.Y. wrote the manuscript, and all authors discussed the results and contributed to revisions.

Additional information

Supplementary information accompanies this paper at <http://www.nature.com/scientificreports>

Competing financial interests: The authors declare no competing financial interests.

How to cite this article: Yang, Z. *et al.* Cobalt monoxide-doped porous graphitic carbon microspheres for supercapacitor application. *Sci. Rep.* **3**, 2925; DOI:10.1038/srep02925 (2013).



This work is licensed under a Creative Commons Attribution-NonCommercial-NoDerivs 3.0 Unported license. To view a copy of this license, visit <http://creativecommons.org/licenses/by-nc-nd/3.0>